Eurographics Symposium on Geometry Processing (2005)
M. Desbrun, H. Pottmann (Editors)

Setting the Boundary Free: A Composite Approach to Surface Parameterization

Rhaleb Zayer, Christian Rössl, and Hans-Peter Seidel

Max-Planck-Institut für Informatik, Saarbrücken, Germany

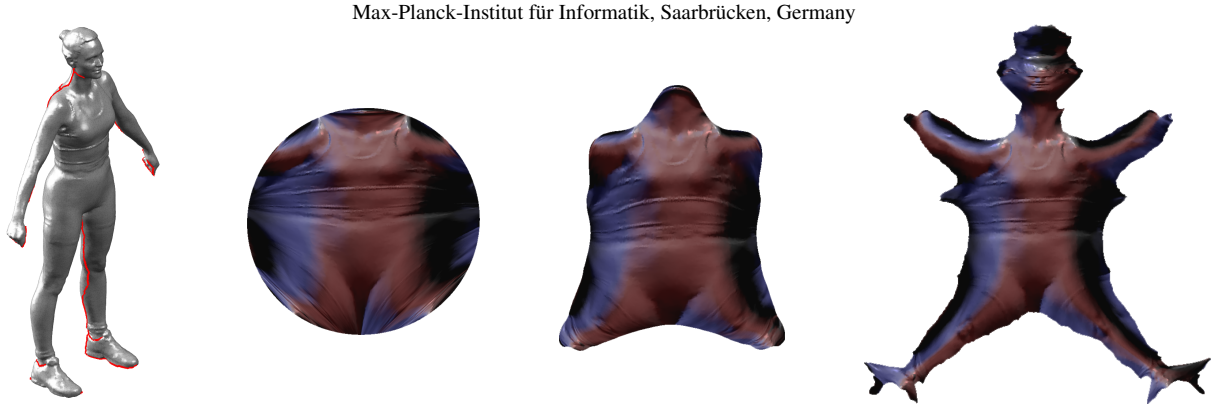

Figure 1: Boundary-free parameterization of a human model (66K△). From left: surface mesh with cut highlighed, initial discrete conformal map, boundary-free conformal map, and boundary-free quasi-harmonic map.

Abstract

In the last decade, surface mesh parameterization has emerged as a standard technique in computer graphics. The ever increasing need for processing large and highly detailed data sets fosters the development of efficient parameterization techniques that can capture the geometry of the input meshes and produce low distortion planar maps. We present a set of novel techniques allowing for low distortion parameterization. In particular, we address one of the major shortcomings of linear methods by allowing the parametric representation to evolve freely on the plane without any *fixed boundary vertices. Our method consists of several simple steps, each solving a linear problem. Our results exhibit a fair balance between high-quality and computational efficiency.*

1. Introduction

Surface mesh parameterization come a standard technique in digital geometry processing which benefits a wide range of applications in computer graphics and simulation. The primary task of parameterization methods is to establish a planar embedding of disk like surface patches. Depending on the application, the embedding is used with different goals and purposes. However, the reduction of angle and area distortion remain the two principal principal aims of most surface mapping techniques. The construction of angle preserving embedding is a fairly well-understood problem, especially in the case of discrete conformal maps which lead to a linear setting. On the other hand, the reduction of both, area and angle distortion, is still a challenging problem. The existing non-linear methods addressing this issue usually lead to intricate and computationally expensive numerical schemes.

In this paper, we present novel techniques for surface parameterization which rely on solving linear systems only. In particular, we address one of the major shortcomings of linear methods by allowing the parametric representation to evolve freely on the planar domain without *any* fixed boundary vertices. So far, linear methods need to fix at least two boundary vertices, where the choice of vertices is not obvious in practice and may affect the result to a large extent especially for surfaces with geometrically complex boundaries.

Based on geometric distortion tensors and general elliptic

partial differential equations, we lay out the theoretical foundation of our approach and derive the ensuing linear optimization problems. Our results reflect a fair balance between high-quality parameterization and computational efficiency.

1.1. Motivation and Overview

Our approach has been motivated by the following two questions:

- How can we quantify the geometric distortion induced by a convex boundary discrete conformal map?
- How can we use this information for establishing a boundary-free parameterization?

We show that a fixed boundary conformal map has all the information necessary for allowing a flat mesh to evolve freely in the plane towards a configuration exhibiting less boundary distortion.

Our method proceeds in a series of simple steps, each involving the solving of a linear problem. We can briefly summarize these steps as follows:

1. For a surface $\mathcal{S}$ compute an initial parameterization $\mathcal{P}_0$, preferably a conformal map with fixed boundary (Fig. 1, center left).
2. Establish a new parameterization $\mathcal{P}_1$ such that $\mathcal{P}_0 \rightarrow \mathcal{P}_1$ is a conformal map, where the image boundary tends to roughly mimic the original boundary of $\mathcal{S}$ (Fig. 1, center right).
3. To further improve the shape of the boundary such that geometric details of the original are captured and to reduce distortion, construct a new map $\mathcal{P}_2$, based on a variant of quasi-harmonic maps (Fig. 1, right).
4. In an optional step, $\mathcal{P}_2$ can be further improved upon by fixing its current boundary and applying discrete tensorial quasi-harmonic maps.

The core of this novel framework consists of steps 2. and 3., which allow the boundary to evolve freely without any constraints. This is achieved by combining distortion tensors with Poisson equations in a manner that treats all – inner and boundary – vertices the same way.

1.2. Background

Within the last decade, parameterization techniques have emerged as an important tool in geometry processing, a fact which is reflected by the significant amount of research on the topic. In the following, we briefly overview the related work, emphasizing free boundary methods. We refer to [FH05] for a more general survey.

Parameterization methods generally flatten a surface (patch) onto a planar parameter domain. A common approach is the explicit minimization of a certain deformation energy in order to control the distortion. The associated numerical problems are often of non-linear type, e.g.,[DMK03, HG00, SSGH01, SdS00, SCGL02, ZMT05, YBS04], and considerable effort is dedicated to the development of efficient numerical solvers. On the other hand, an elegant alternative which preserves angles relies on the solution of the Laplace equation which yields the discrete conformal maps [EDD*95, HAT*00, PP93, DMA02, LPRM02, GY03]. Variants of this linear setting propose alternative discretizations of the Laplace-Beltrami operator [Flo97, Gus02, SdS02, Flo03].

In general, the boundary shape in the parametric domain has a significant influence on the overall distortion. Therefore it is crucial to take it into account in the parameterization setup in order to reflect the geometry of the original surface patch.

The most prominent approach to surface parameterization which features a freely evolving boundary is the angle based flattening (ABF) [SdS00]. The minimization problem is specified in terms of inner angles, and in particular there are no constraints on the boundary. ABF generates pseudo-conformal maps, where the initial method has been further developed, e.g., most recently applying efficient and robust non-linear optimization [SLMB05].

Linear methods usually apply a convex Dirichlet-type boundary. [LKL02] embed the surface patch in a larger one by heuristically growing a "virtual boundary" which to some extent absorbs distortion induced by the convex boundary setting. (Similarly, the non-linear approach in [ZMT05] applies virtual boundaries in combination with "scaffolding triangles".) Alternatively, [DMA02, LPRM02] apply Neumann boundary conditions which only require fixing (at least) two boundary vertices. [SLMB05] note that in practice, unsatisfactory results are often obtained for geometrically complex boundaries. [KGG05] discuss the design of such boundary conditions in the presence of constraints.

Our approach is partly based on discrete tensorial quasi-harmonic maps [ZRS05]. These maps rely on linear operators that capture parametric distortion in the form of local deformation tensors in contrast to scalar weights (as applied in [YBS04] for example).

Here, such tensors are used as guidance fields in a way similar to the Poisson equation settings used recently in image editing [PGB03] and mesh editing [YZX*04] scenarios.

The remainder of this paper is organized as follows. Sec. 2 reviews the general differential setting for the different maps, which are introduced as basic tools in Sec. 3 (conformal maps) and Sec. 4 (quasi-harmonic maps). In Sec. 5, we show how these tools are combined for boundary-free parameterization. Results are presented in Sec. 6 along with a discussion, and Sec. 7 concludes the paper.

2. General Differential Setting

We briefly summarize the notation and present the general differential framework used in the subsequent sections.

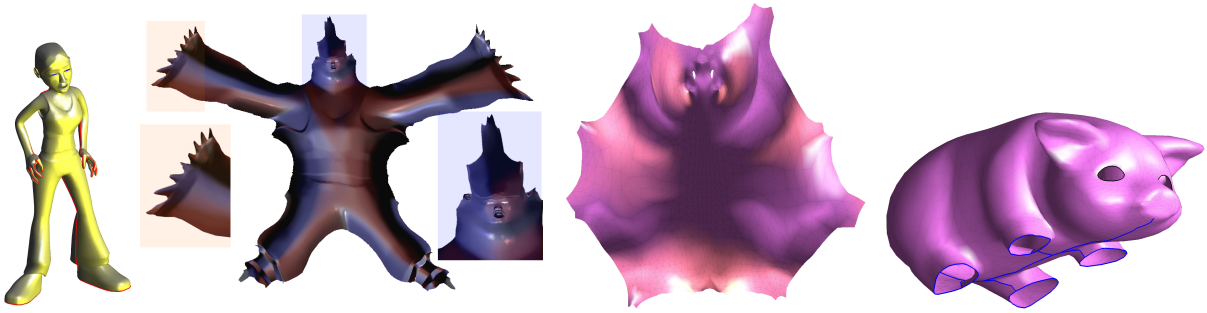

Figure 2: *Mapping another (four-fingered) human model (20K△) and a pig (4K△) model to the plane. For both, the eyes are holes, which do not require any special treatment.*

We consider surfaces homeomorphic to a disk, possibly with holes. A triangular surface mesh $\mathcal{S}$ is described as the pair $(\mathcal{K},S)$, where $\mathcal{K}$ is a simplicial complex representing the connectivity of vertices, edges and faces, and $S=(X_1,\ldots,X_n)$, where $X_k\in\mathbb{R}^3$ refer to the geometric positions of the vertices.

We represent a *parameterization* of a surface as an isomorphic mesh $\mathcal{U}=(\mathcal{K},(U_1,\cdots,U_n))$, where $U_k=(u_k,v_k)^\top\in\mathbb{R}^2$, $1\leq k\leq n$, denotes positions in the (planar) parameter domain.

We define the *1-ring neighborhood* of a vertex $i\in\mathcal{K}$ as the set of adjacent vertices $\mathcal{N}_i=\{j|(i,j)\in\mathcal{K}\}$ directly connected to i by an edge.

In the following sections, we will consider the steady-state elliptic equation

$$\mathbf{div}(\mathbf{C}\,\mathbf{grad}u) \;=\; f$$

with appropriate boundary conditions. $\mathbf{C}$ is a piecewise constant field of 2×2 tensors, i.e. each triangle $j\in\mathcal{K}$ is associated with a local tensor $\mathbf{C}_j$. For the identity $\mathbf{C}\equiv\mathbf{Id}$, this reduces to the well-known (Dirichlet problem for the) *Laplace equation* when $f\equiv 0$ and the *Poisson equation* when f is a non-null function.

The discretization of this setting is well-known in general and leads to a sparse symmetric linear system

$$Lu \;=\; b\,. \tag{1}$$

For the case of *discrete conformal maps* consider a triangle $T_j=\{i,j,j+1\}$. Then the local contribution of half-edge $\{i,j\}$ to the matrix L is given by

$$w_{ij}^{T_j} \;=\; \frac{\mathbf{x}_{j+1,j}^{\perp}\mathbf{C}_j\cdot\mathbf{x}_{i,j+1}^{\perp}}{4A_j}\,, \tag{2}$$

where $\mathbf{x}_{i,j+1}^{\perp}$ refers to the edge rotated by $\frac{\pi}{2}$ (see Fig. 3), and hence the contribution of the full edge is

$$\begin{aligned} w_{ij} \;&=\; w_{ij}^{T_{j-1}}+w_{ij}^{T_j} \\ &=\; \frac{\mathbf{x}_{j-1,i}^{\perp}\mathbf{C}_{j-1}\cdot\mathbf{x}_{j,j-1}^{\perp}}{4A_{j-1}}+\frac{\mathbf{x}_{j+1,j}^{\perp}\mathbf{C}_j\cdot\mathbf{x}_{i,j+1}^{\perp}}{4A_j}\,. \end{aligned} \tag{3}$$

For $\mathbf{C}\equiv\mathbf{Id}$ these are the well-known cotangent weights [PP93, DMA02, LPRM02]. For details on this discretization, we refer to [ZRS05], where in addition a similar generalization of the mean value coordinates [Flo03] is proposed which can be used alternatively. In our context, where the support of the differential operator is restricted to the 1-ring of a vertex, the parameterization problem reduces to a linear system of following type

$$\mathcal{L}(U_i)=\sum_{j\in\mathcal{N}_i}w_{ij}(U_i-U_j) \;=\; 0\,,\quad i\in\mathcal{K}\,. \tag{4}$$

3. Conformal Maps

Based on the above differential setting, we concisely characterize the different types of maps used as basic tools in our approach. In this section, we start with conformal maps, and we continue with quasi-harmonic maps in Sec. 4.

3.1. Prescribed-boundary Conformal Maps

Linear parameterization schemes proceed by solving the Laplace equation. For the mapping function from the surface to the plane we have

$$\nabla^2 u \;=\; \mathbf{div}(\mathbf{Id}\,\mathbf{grad}u) \;=\; 0\,. \tag{5}$$

Given appropriate Dirichlet conditions on the boundary, the resulting parameterization is guaranteed to be a one-to-one mapping. The parameterization depends closely on the choice of weights used for the discrete operator $\mathcal{L}$ in (4). In practice, the cotangent weights (i.e., (3)) or the mean value coordinates [Flo03] are used with a fixed convex boundary, e.g., the boundary is fixed to a circle.

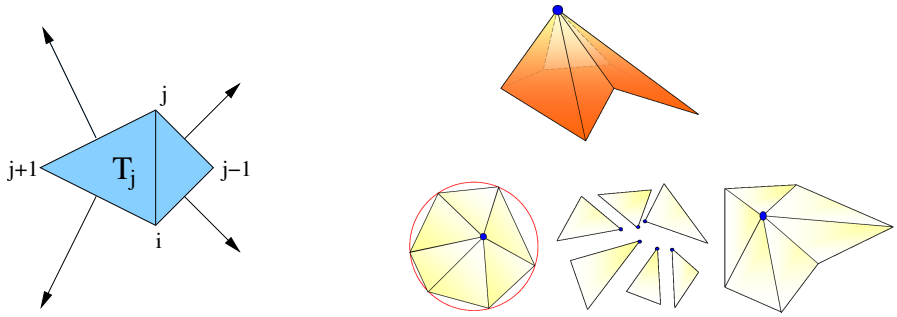

(a) (b)

Figure 3: *(a) The two triangles adjacent to edge $\{i, j\}$. The outward vectors $\mathbf{x}^{\perp}$ correspond to respective edges rotated by $\frac{\pi}{2}$. (b) Poisson setting on a 1-ring: Starting from the 3D surface, a prescribed convex boundary discrete conformal map is established. The tensor field $\mathbf{C}$ is computed from this map and then applied to the linear pieces of the flat configuration. The triangles of the discontinuous setting show less distortion and are used to setup the right hand side of the Poisson equation. The solution is a (continuous) boundary-free conformal map.*

3.2. Boundary-free Conformal Maps

Solving the Laplace equation with Dirichlet boundary conditions is an extremely efficient way to establish a conformal map from the plane to the surface. The fixed boundary however does not necessarily respect the geometry of the original mesh as illustrated, e.g., in Fig. 1, center left. In order to improve the boundary shape, [DMA02, LPRM02] fix a small (≥ 2) number of boundary points and impose certain local equations on the rest of the boundary. [LPRM02] derive an alternative formulation of these equations from the Cauchy-Riemann equations. Although most boundary vertices are "free", the solution is sensitive to the choice of the fixed vertices. For geometrically simple boundaries, satisfactory results are obtained. For more complex boundary shapes, the results may suffer from considerable distortion or the solution might even be invalid as the flat mesh does not unfold correctly (see, e.g., [SLMB05] who partially motivate their non-linear ABF++ method by this fact). Virtual boundary methods [LKL02] allow for additional degrees of freedom and provide an interesting alternative but do not seem to always provide a satisfactory solution due to the limited effect of padding with virtual vertices (see also [KGG05]).

Our approach is motivated by the Poisson equation. So, instead of letting boundary conditions dictate the behavior of the whole solution, we aim at specifying the same type of conditions over the whole mesh. Hence, all vertices are treated in a similar manner, and boundary distortion is reduced simultaneously with the overall distortion.

For modeling this problem, we have to correctly specify the right hand side b of the Poisson equation (1). More formally, we are looking for a suitable vector field F, which can be used as a guidance field for the partial differential equation

$$\nabla^2 u \;=\; \mathbf{div} F \;. \tag{6}$$

We note that unlike the Laplace equation, here, the right hand side is specified for *all* vertices including boundary points as well. We refer to [PGB03, YZX*04] for a discussion of this type of equation in the context of computer graphics.

The solution of (6) is very sensitive to the guidance field F and thus a meticulous setup of this field is de rigueur. Since our aim is to reduce the distortion of the planar configuration, it seems natural to characterize the right hand side in terms of an initial prescribed boundary conformal map. Most recently, [ZRS05] introduced a piecewise constant tensor field that locally mimics the Jacobian of the map from a given planar configuration to the surface in 3D. This tensor comes in handy as it is a key ingredient for our Poisson equation setup.

Given an initial conformal map, we define such 2×2 tensors $\mathbf{C}_j$ per triangle $j \in \mathcal{K}$, i.e.,

$$\mathbf{C}_j \;=\; (\mathbf{J}_j{}^{\top} \mathbf{J}_j)^{\frac{1}{2}} \;,$$

where $\mathbf{J}_j$ denotes the 3×2 Jacobian of the initial map. We refer to [ZRS05] for details on the derivation of the tensor field $\mathbf{C}$. In contrast to the latter we *apply* the tensor field here *directly* to the planar configuration.

So for every triangle we get $T'_j = \mathbf{C}_j\, T_j$, i.e., this intermediate step can be imagined as splitting mesh triangles apart resulting in a geometrically fragmented mesh whose vertices are three times the number of triangles of the original. Fig. 3 illustrates the local situation for a 1-ring. Now considering

the new coordinates as scalar fields over the initial parameterization, we obtain the right hand side $b := \mathbf{div}F$ of (6) as follows. We compute the gradient per triangle on the discontinuous mesh using the discretization (2). The divergence of this gradient field is summed at vertices shared between triangles according to the original mesh connectivity, yielding the right hand side vector b. In other words, the Laplacian of the fragmented mesh is first computed and then applied to the coordinates of the fragmented mesh. The resulting coordinates are summed according to the original connectivity, which provides the per-vertex components of b.

4. Quasi-Harmonic Maps

Quasi-harmonic maps are the second tool used in our approach. This type of maps has been introduced for prescribed boundary parameterization in [ZRS05], and here we take advantage of their properties for our boundary-free setting.

4.1. Prescribed-boundary Quasi-Harmonic Maps

Discrete tensorial quasi-harmonic maps can account for distortion away from the boundary. The approach attempts to reduce the distortion by minimizing the quasi-harmonic energy functional

$$\int_{\Omega} (\mathbf{C}\nabla f) \cdot (\nabla f) \, ,$$

where the tensor field $\mathbf{C}$ is defined as in Sec. 3.2. The partial differential equation associated with this energy is the quasi-harmonic equation

$$\mathbf{div}(\mathbf{C}\,\mathbf{grad} f) \;=\; 0 \, . \tag{7}$$

Quasi-harmonic maps establish planar maps which mimic the original three dimensional shape not only in angles but also in area as $\mathbf{C}$ captures the properties of the Jacobian of the initial map.

4.2. Boundary-free Quasi-Harmonic maps

So far, quasi-harmonic maps have only been applied to fixed boundaries. Building upon the Poisson setting of Sec. 3.2, we can easily extend the method to completely boundary-free parameterization.

Starting from boundary-free conformal maps, we aim to further improve it. This can be achieved by applying a variant of the quasi-harmonic maps but in the more general Poisson setting. Here, we solve the following differential equation

$$\mathbf{div}(\mathbf{C}\,\mathbf{grad} u) \;=\; \mathbf{div}F \, . \tag{8}$$

This formula differs from (7) only in the right hand side, which is computed similarly to the Poisson setting (6). Hence, we have now all tools necessary to set up the linear systems for the boundary-free maps.

5. Overall Method

In the previous sections, we described all ingredients required for our approach. Now putting it all together, the overall method reads simply as sketched in Sec. 1.1. We proceed in several steps, each step corresponds to one of the previously described differential settings.

In the first step, an initial *prescribed-boundary conformal map* (cf. Fig. 1, center left) is constructed in the standard way by solving the Laplace equation (5) with fixed convex boundary, e.g., using a circle.

To let the boundary evolve freely, a *boundary-free conformal map* (cf. Fig. 1, center right) is established as a second step. Here, the guidance tensor field for the setup of the Poisson equation (6) is obtained from the Jacobian of the initial mapping.

The resulting planar configuration is generally non-convex and tends to roughly mimic the shape of the 3D boundary, however, it fails to capture completely the full detail of the original surface boundary. In order to further improve it, a *boundary-free quasi-harmonic map* is constructed from (8) (cf. Fig. 1, right) this time the tensor field is computed based on the previous boundary-free conformal parameterization. The boundary of the consequent parameterization resembles its 3D counterpart much more closely.

Optionally, the result can be further improved by fixing the boundary and solving (7) for a *prescribed-boundary quasi-harmonic map*, which is exactly the formulation of discrete tensorial quasi-harmonic maps [ZRS05]. We note that in this last step the role of the tensor field is restricted compared to the previous steps.

Finally, we note that there is no loop or iteration in this process, each step is carried out once, solving only one single sparse symmetric linear system. We refer to [BBK05] for a recent overview on efficient solving strategies for these type of linear problems. In particular, the following properties can be exploited: The two initial (discrete conformal) steps apply the same linear operator ∇^2, i.e., one can easily reuse for instance a Cholesky factorization of the system matrix and hence obtain the second map simply by back-substitution. Note that this is not possible for the subsequent (quasi-harmonic) steps, as different tensor fields are applied. However, one still can take advantage of a symbolic factorization, which depends only on the mesh connectivity, over all the four steps.

6. Results and Discussion

We applied our approach to a variety of surface meshes with non-trivial boundaries. In fact, most models were cut explicitly to make any parameterization method feasible. Results are shown in Figures 1, 2, 4, 5, 7-10, some with the cuts highlighted for the 3D surfaces. The maps are visualized as

flat meshes rendered with the original shading and/or as texture maps. In all our tests, the resulting maps are valid, i.e., bijective with no triangle foldovers. However, currently we cannot claim any general validity properties of our approach. Some of the models contain holes, they were processed as is with no special treatment necessary. The size of the models is indicated for every example, and it is generally in the order of tens of thousands of triangles. Note that the mapping is inherently independent of the particular tessellation and resolution. The runtime for solving the linear systems is in the order of a few seconds for all examples, we refer to the previous section for remarks on efficient solution strategies. Furthermore, for these kind of problems multi-grid grid methods are well-understood and readily available as standard tools to process even very large input. The current results neither require nor apply a supporting hierarchy, either for robustness or for efficiency. In addition, we remark that the implementation of our method is straightforward. Any existing implementation of linear parameterization can be extended with only little effort to confirm our results.

As mentioned before, linear methods with Neumann-type boundary conditions do not always lead to valid solutions [SLMB05], in particular this applies to many of the surfaces shown here. However, we note that with careful choice of (eventually more than two) fixed vertices the method often produces good results solving a single linear system. It is hard to quantify this aspect as the approach is sensitive to this choice as illustrated for a simple model in Fig. 9. (A non-linear alternative based on Green's functions remedies this problem for small boundaries [DMA02].)

We therefore compare our approach to non-linear angle based flattening (ABF) [SdS00, SLMB05]. Figure 6 compares the distortion of angles and triangle areas (vertical axis) plotted over the sequence of faces as they appear in the data set (horizontal axis), i.e., distortion on every triangle is visualized. The optimal ratio indicating no distortion is 1.

The diagram shows that ABF produces high quality maps as expected, and that we come close. Note that for both methods the results depend largely on boundaries or choice of cuts, respectively. For the horse model (Fig. 5), we use the original cut of [SLMB05], and our result is still competitive. Of course, there must be tradeoffs between the efficiency and simplicity of our linear setting against the high quality of the non-linear ABF. We think, that our approach provides a fair balance between the computational efficiency of establishing discrete conformal maps and the free boundary ABF.

Finally, we address limitations of our approach. As mentioned before, the boundary path resulting from cutting surfaces to disk-like patches affects parameterization methods. For all our cuts we used simple Dijkstra shortest paths joining a set of marked vertices. Where indicated in the examples, we use the cuts from from [SLMB05]. Our method depends largely on the initial prescribed boundary conformal map. If there are nearly degenerate triangles (very small area) in the flat mesh, then there might be an overreaction in the subsequent steps, i.e., these triangles may end up having large areas in the boundary-free maps. This may happen for long cuts traversing a relatively small surface area (or more figuratively, volume). In fact, for the initial arc-length parameterization of the fixed boundary over the circle, such triangles will cover a large perimeter and will be extremely distorted. Fig. 8 shows an example, the tail of the camel ends up having an area comparable to the legs. This situation could be greatly improved by optimizing the cut or using a suitable re-parameterization of the initial convex boundary curve.

7. Conclusions

We presented a boundary-free parameterization method consisting of few simple steps. The overall process is controlled using suitable guidance tensor fields reflecting the intrinsic surface geometry. The arising linear systems are symmetric and of similar structure, i.e., the maps can be computed robustly and efficiently.

Our results confirm that despite their simplicity, methods based purely on linear settings have the potential to produce high-quality boundary-free parameterizations, a goal that was only partially met by prior linear methods. We cannot claim the optimality of our results, however, we observe a fair compromise between quality and efficiency and hope that this work will stimulate more research towards pushing the limits of linear parameterization. Future work directions include the suppression of artifacts induced by improper cuts.

Acknowledgements

The authors would like to thank Alla Sheffer for providing the balls model and the cut horse and camel models along with the corresponding ABF parametric coordinates.

This work was partly supported by the EU Project AIM@SHAPE (Contract # 506766).

References

[BBK05] BOTSCH M., BOMMES D., KOBBELT L.: Efficient linear system solvers for mesh processing. In *11th IMA Conference on the Mathematics of Surfaces (preprint)* (2005). 5

[DMA02] DESBRUN M., MEYER M., ALLIEZ P.: Intrinsic parameterizations of surface meshes. *Computer Graphics Forum (Proc. Eurographics) 21*, 3 (2002), 209–218. 2, 3, 4, 6, 9

[DMK03] DEGENER P., MESETH J., KLEIN R.: An adaptable surface parameterization method. *Proc. 9th International Meshing Roundtable* (2003), 201–213. 2

Figure 4: *Subsequent maps of the gargoyle model (20K△). From left: prescribed boundary conformal map, boundary-free conformal-map, boundary-free quasi-harmonic, improvement by prescribed boundary quasi-harmonic maps.*

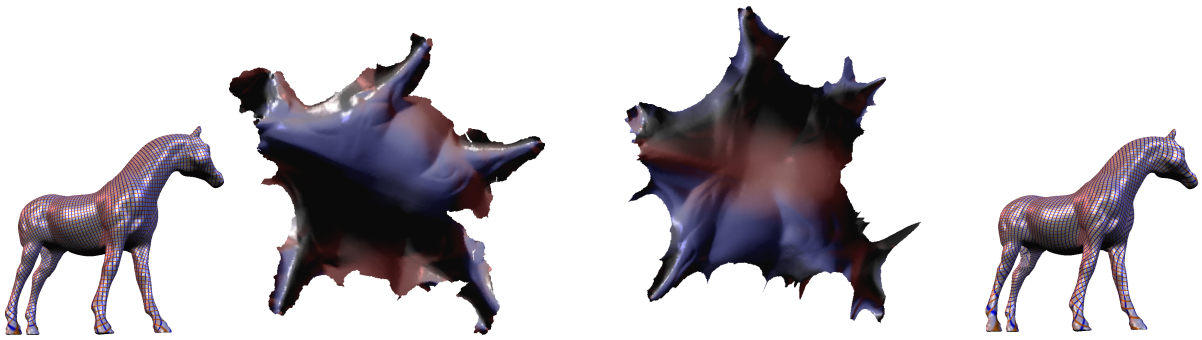

Figure 5: *Comparing maps of the horse model (40K△, original cut of [SLMB05]). Left: ABF. Right: Our method.*

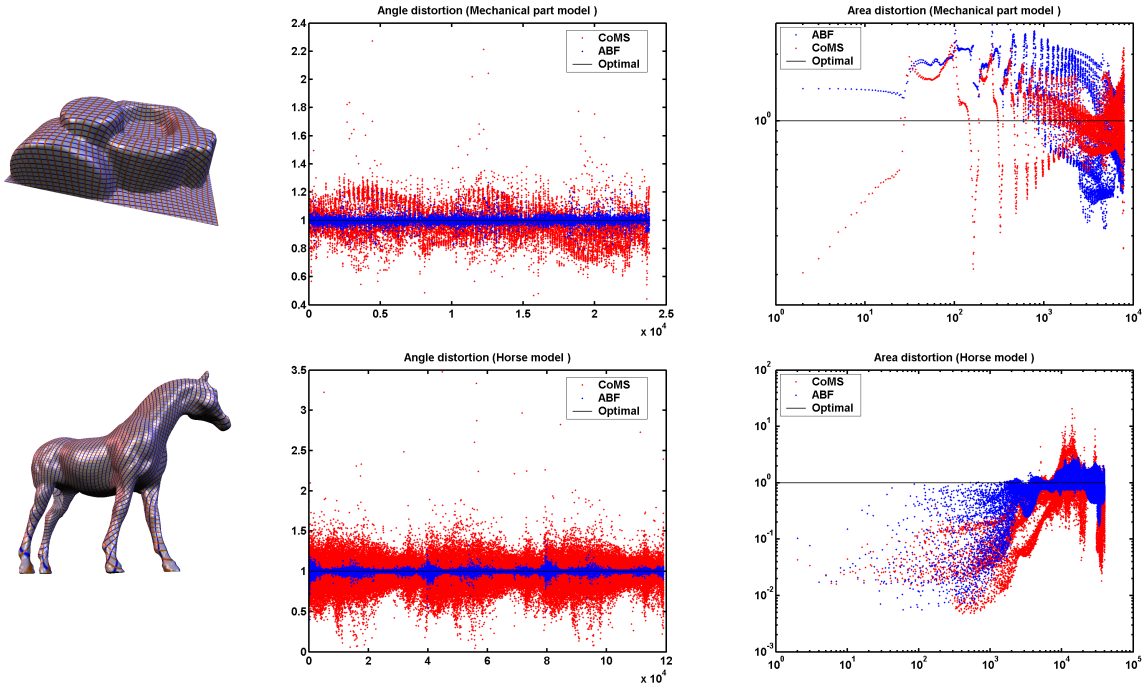

Figure 6: *Distortion of angles (center column) and triangle areas (right column, log-scale) for the mechpart and the horse model using the original cut of [SLMB05]. Blue: ABF. Red: our method.*

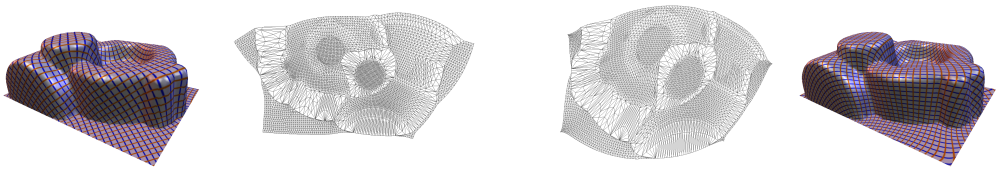

Figure 7: *Maps of the mechpart (8K△). Left: ABF. Right: Our method.*

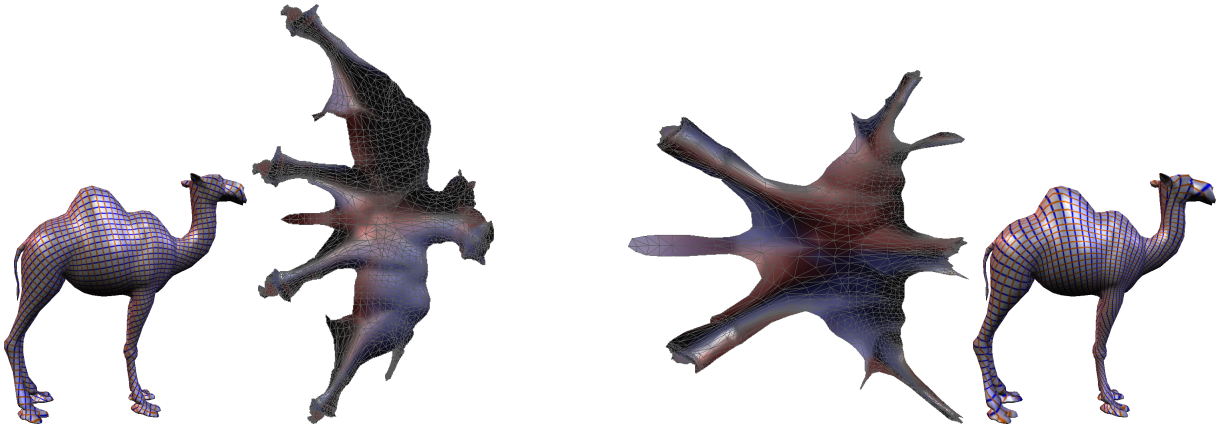

Figure 8: *Mapping the camel model (4k△, original cut of [SLMB05]). Left: ABF. Right: Our method. For the tail, the system overreacts due to extreme distortion for the initial prescribed boundary conformal map.*

[EDD*95] ECK M., DEROSE T., DUCHAMP T., HOPPE H., LOUNSBERY M., STUETZLE W.: Multiresolution analysis of arbitrary meshes. *Computer Graphics (Proc. SIGGRAPH) 29* (1995), 173–182. 2

[FH05] FLOATER M. S., HORMANN K.: Surface parameterization: a tutorial and survey. In *Advances in Multiresolution for Geometric Modelling*, Dodgson N. A., Floater M. S.,, Sabin M. A., (Eds.), Mathematics and Visualization. Springer, Berlin, Heidelberg, 2005, pp. 157–186. 2

[Flo97] FLOATER M. S.: Parametrization and smooth approximation of surface triangulations. *Computer Aided Geometric Design 14*, 3 (1997), 231–250. 2

[Flo03] FLOATER M. S.: Mean value coordinates. *Computer Aided Geom. Design 20*, 1 (2003), 19–27. 2, 3

[Gus02] GUSKOV I.: An anisotropic mesh parameterization scheme. In *IMR* (2002), pp. 325–332. 2

[GY03] GU X., YAU S.-T.: Global conformal parameterization. In *Proc. Symposium on Geometry processing* (2003), pp. 127–137. 2

[HAT*00] HAKER S., ANGENENT S., TANNENBAUM A., KIKINIS R., SAPIRO G., HALLE M.: Conformal surface parameterization for texture mapping. *IEEE Transactions on Visualization and Computer Graphics 6*, 2 (2000), 181–189. 2

[HG00] HORMANN K., GREINER G.: MIPS: An efficient global parametrization method. In *Curve and Surface Design: Saint-Malo 1999*, Laurent P.-J., Sablonnière P.,, Schumaker L. L., (Eds.). Vanderbilt University Press, 2000, pp. 153–162. 2

[KGG05] KARNI Z., GOTSMAN C., GORTLER S. J.: Free-boundary linear parameterization of 3d meshes in the presence of constraints. In *Shape Modeling International (preprint)* (2005). 2, 4

[LKL02] LEE Y., KIM H. S., LEE S.: Mesh parameterization with a virtual boundary. *Computers & Graphics 26*, 5 (2002), 677–686. 2, 4

[LPRM02] LÉVY B., PETITJEAN S., RAY N., MAILLOT J.: Least squares conformal maps for automatic texture atlas generation. *ACM Transactions on Graphics (Proc. SIGGRAPH) 21, 3* (2002), 362–371. 2, 3, 4

[PGB03] PÉREZ P., GANGNET M., BLAKE A.: Poisson image editing. *ACM Transactions on Graphics (Proc. SIGGRAPH) 22*, 3 (July 2003), 313–318. 2, 4

[PP93] PINKALL U., POLTHIER K.: Computing discrete minimal surfaces and their conjugates. *Experiment. Math. 2*, 1 (1993), 15–36. 2, 3

[SCGL02] SORKINE O., COHEN-OR D., GOLDENTHAL R., LISCHINSKI D.: Bounded-distortion piecewise mesh

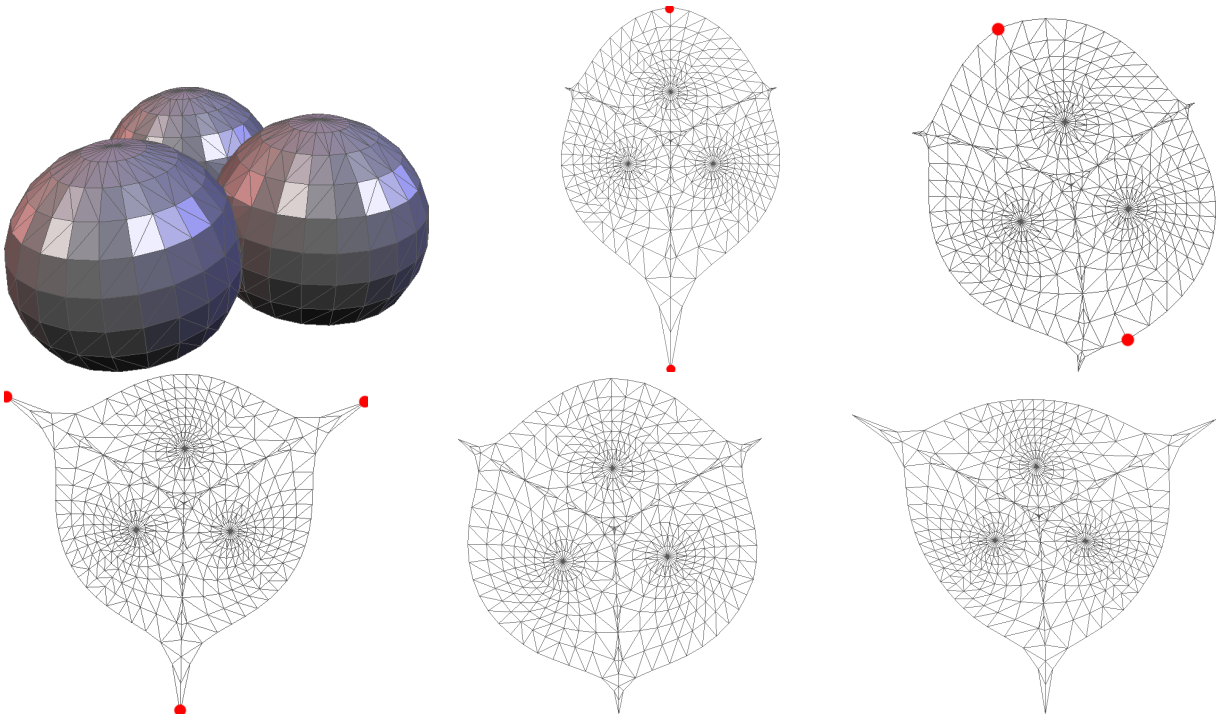

Figure 9: *Mapping the balls model (top left, 1300△), using [DMA02] fixing different boundary vertices depicted in red. We compare to the results of ABF (bottom center) and our method (bottom right).*

parameterization. In *Proc. IEEE Visualization* (2002), pp. 355–362. 2

[SdS00] SHEFFER A., DE STURLER E.: Parameterization of faceted surfaces for meshing using angle based flattening. *Engineering with Computers 17*, 3 (2000), 326–337. 2, 6

[SdS02] SHEFFER A., DE STURLER E.: Smoothing an overlay grid to minimize linear distortion in texture mapping. *ACM Transactions on Graphics 21*, 4 (2002), 874–890. 2

[SLMB05] SHEFFER A., LEVY B., MOGILNITSKY M., BOGOMYAKOV A.: ABF++ : Fast and robust angle based flattening. *ACM Transactions on Graphics (preprint)* (2005). 2, 4, 6, 7, 8

[SSGH01] SANDER P. V., SNYDER J., GORTLER S. J., HOPPE H.: Texture mapping progressive meshes. In *Computer Graphics (Proc. SIGGRAPH)* (2001), pp. 409–416. 2

[YBS04] YOSHIZAWA S., BELYAEV A. G., SEIDEL H.-P.: A fast and simple stretch-minimizing mesh parameterization. In *Proc. Shape Modeling International* (2004), pp. 200–208. 2

[YZX*04] YU Y., ZHOU K., XU D., SHI X., BAO H., GUO B., SHUM H.-Y.: Mesh editing with Poisson-based gradient field manipulation. *ACM Transactions on Graphics (Proc. SIGGRAPH) 23*, 3 (2004), 644–651. 2, 4

[ZMT05] ZHANG E., MISCHAIKOW K., TURK G.: Feature-based surface parameterization and texture mapping. *ACM Transactions on Graphics 24*, 1 (2005), 1–27. 2

[ZRS05] ZAYER R., RÖSSL C., SEIDEL H.-P.: Discrete tensorial quasi-harmonic maps. In *Shape Modeling International (preprint)* (2005). 2, 3, 4, 5

Figure 10: *More maps computed with our method: The head model (16K△) self-intersects in 3D, the flat mesh shows no foldovers. Dinosaur (48K△). Double torus (2K△). Holes like the windows of the beetle model (2K△) do not require any special treatment. Santa (114K△).*